

This discussion paper is/has been under review for the journal Hydrology and Earth System Sciences (HESS). Please refer to the corresponding final paper in HESS if available.

Soil erosion areas in the Blue Nile-Eastern Sudan

M. El Haj El Tahir et al.

Identification and mapping of soil erosion areas in the Blue Nile-Eastern Sudan using multispectral ASTER and MODIS satellite data and the SRTM elevation model

M. El Haj El Tahir, A. Käab, and C.-Y. Xu

Department of Geosciences, University of Oslo, P.O. Box 1047 Blindern, 0316 Oslo, Norway

Received: 2 December 2009 – Accepted: 11 December 2009 – Published: 12 January 2010

Correspondence to: M. El Haj El Tahir (majdulie@ulrik.uio.no)

Published by Copernicus Publications on behalf of the European Geosciences Union.

Title Page

Abstract

Introduction

Conclusions

References

Tables

Figures

◀

▶

◀

▶

Back

Close

Full Screen / Esc

Printer-friendly Version

Interactive Discussion



Abstract

This paper is part of a set of studies to evaluate the spatial and temporal variability of soil water in terms of natural as well as land-use changes as fundamental factors for vegetation regeneration in arid ecosystems in the Blue Nile-Sudan. The specific aim is to indicate the spatial distribution of soil erosion caused by the rains of 2006. The current study is conducted to determine whether automatic classification of multispectral Advanced Space borne Thermal Emission and Reflection Radiometer (ASTER) imagery could accurately discriminate erosion gullies. Shuttle Radar Topography Mission (SRTM) is used to orthoproject ASTER data. A maximum likelihood classifier is trained with four classes, Gullies, Flat.Land, Mountains and Water and applied to images from March and December 2006. Validation is done with field data from December and January 2006/2007, and using drainage network analysis of SRTM digital elevation model. The results allow the identification of erosion gullies and subsequent estimation of eroded area. Consequently the results were up-scaled using Moderate Resolution Imaging Spectroradiometer (MODIS) images of the same dates. Because the selected study site is representative of the wider Blue Nile province, it is expected that the approach presented could be applied to larger areas.

1 Introduction

This paper is the second (the first is Xu et al., 2009) in a set of studies to evaluate the spatial and temporal variability of soil water in terms of natural factors as well as land-use changes as fundamental factors for vegetation regeneration in arid ecosystems in the Blue Nile-Eastern Sudan. This study is concerned with evaluating the spatial distribution of soil erosion as one of the implications of climate and land-use changes in the study region. Such an evaluation of soil degradation is regarded as an important initial inventory in order to further assess its soil water content status (Gomer and Vogt, 2000). Erosion can be a result of anthropogenic disturbance such as overgrazing, soil

Soil erosion areas in the Blue Nile-Eastern Sudan

M. El Haj El Tahir et al.

Title Page

Abstract

Introduction

Conclusions

References

Tables

Figures

◀

▶

◀

▶

Back

Close

Full Screen / Esc

Printer-friendly Version

Interactive Discussion



crust disturbance, and global climatic changes that increase ambient temperature and reduce or increase precipitation. Reduction of precipitation causes reduction of plant growth and consequently leads to increases in erosion rates. Similarly, increasing precipitation can also be a climate change result, and can enhance erosion as well (Crawford and Gosz, 1982; Evenari et al., 1982; Schlesinger et al., 1996). Or it could happen as a natural process. It is important to differentiate between natural and anthropogenic causes of erosion because we have little control over the former process. Only once natural and anthropogenic sources of erosion have been differentiated will it be possible to develop adequate erosion control policies against anthropogenic erosion. The most important factors controlling erosion are rainfall regime, vegetation cover, terrain slope and soil type (Linsley et al., 1982). Fluctuating rainfall amounts and intensities have significant impacts on soil erosion rates. Where rainfall amounts increase, erosion and runoff increase at an even greater rate. Decreasing annual rainfall triggers system feedbacks related to the decreased biomass production that lead to greater susceptibility of the soil to erode (Nearing et al., 2004). Because of the important role of direct rain drop impact, vegetation provides significant protection against erosion by absorbing the energy of the falling drops and generally reducing the drop sizes, which reach the ground. Vegetation may also provide mechanical protection to the soil against gully erosion via the root system. In addition, an adequate vegetation cover generally improves infiltration through the addition of organic matter to the soil. Higher infiltration capacity means less overland flow and consequently less erosion potential. Rates of erosion are greater on steep slopes than on flat slopes. The steeper the slope the more effective splash slope erosion is in moving soil down slope. Overland flow velocities are also greater on steep slopes, and mass movements are more likely to occur in steep terrain. Length of slope is also important. The shorter the slope length, the sooner the eroded material reaches the stream, but this is offset by the fact that overland-flow discharge and velocity increase with length of slope. Land-use is also an important factor in fixing the rate of erosion. Poor cropping practices or careless construction of roads may greatly accelerate erosion. Removal of vegetation by fire or

Soil erosion areas in the Blue Nile-Eastern Sudan

M. El Haj El Tahir et al.

Title Page

Abstract

Introduction

Conclusions

References

Tables

Figures

◀

▶

◀

▶

Back

Close

Full Screen / Esc

Printer-friendly Version

Interactive Discussion



lumbering may also increase the erosion hazard. Proper soil conservation practices may greatly reduce erosion losses.

Arid and semi-arid regions are particularly susceptible to soil erosion due to their low plant cover (Bull, 1981). In time, such soil erosion also results in the loss of soil nutrients, particularly carbon and nitrogen (West, 1991; Mokwunye, 1996), due to the restrictions of feedbacks in carbon and nitrogen cycles between plants, atmosphere and soil (Schlesinger et al., 1990). Considerable literature (Thornes, 1990; Ayoub, 1998; Nakileza et al., 1999; Symeonakis and Drake, 2004) point to the widespread natural resource degradation especially in sub-Saharan Africa, including Sudan. The area of the Upper Blue Nile in Eastern Sudan was considered prone to degradation by (Symeonakis and Drake, 2004). The reasons for this degradation among others are the rapid human population growth placing pressure on land resources through intensive cultivation, and encroachment on marginal lands. Drought, natural or human-induced reduction in vegetation cover, poor agricultural practices leading to soil aggregate breakdown and soil organic matter losses, poor irrigation practices leading to salinization, all lead to an increase in soil erosion rates and, ultimately, desertification. Erosion, therefore, seems to be the single most important indicator of the desertification process.

The objectives of this study are (1) to identify the erosion areas using multispectral satellite images from the Advanced Spaceborne Thermal Emission and Reflection Radiometer ASTER sensor together with field work data and (2) to upscale and map the spatial distribution of soil erosion area changes using Moderate Resolution Imaging Spectroradiometer MODIS.

To achieve these objectives, a qualitative erosion identification and mapping approach is developed in the study based on adaptations to the regional characteristics of the study area and the availability of data.

Soil erosion areas in the Blue Nile-Eastern Sudan

M. El Haj El Tahir et al.

Title Page

Abstract

Introduction

Conclusions

References

Tables

Figures

◀

▶

◀

▶

Back

Close

Full Screen / Esc

Printer-friendly Version

Interactive Discussion



2 Study area and data

2.1 Description of study area

The study area lies between latitudes 10° and 14° N and longitudes 33° and 34° E (Fig. 1). It portrays different land use types including agriculture, forests and range areas. Agriculture forms are small holdings, mechanized and river bank farming. The area is bounded by Sennar town in the north and Ed Damazin town in the south and traversed by the Blue Nile. It exhibits high land cover variability. It includes for example the Ar Roseris power dam and its lake. There are a number of forests for example the Okalma forest reserve which is bound by Jabal Okalma (Jabal is the local Arabic word for mountain) on the west and Jabal Zign (400 m a.s.l.) on the south east corner. Both mountains constitute a source of sheet floods towards the Okalma forest reserve. The forest reserve is a natural forest composed of a mixture of trees, mainly *Acacia seyal* and *Balanites aegyptiaca* plus other species. There is large variation of age groups from young new regeneration to large groups of forest stands following abandonment of agricultural cropping. The forest is related to the surrounding societies providing diversified benefits from the trees and the land. Regeneration and forest development factors are evident. Other areas are abandoned fallow land. To the south-east there is the seasonal *Khor* Dunya (a gully is locally known as *Khor*, the Arabic word for seasonal water course) running from south west to north east until it joins the Blue Nile at a point 35 km north of Ed Damazin town. *Khor* Dunya represents a catchment area with the Ingessana Hills south of the catchment area acting as the source of the *Khor*. Bordering Ed Damazin from south and west is *Khor* Dunya forest reserve, a natural forest composed of a variety of tree species, and traversed by *Khor* Dunya seasonal water. This *Khor* is characterised by the presence of degraded areas, natural regeneration, human activities such as agriculture, pastoralism and small settlements, and human intervention to reclaim the vegetation. Gully erosion stripes off the fertile clay soils from the degradational clay plain forming bad-lands known locally as “Kerib” (Mirghani, 2007).

Soil erosion areas in the Blue Nile-Eastern Sudan

M. El Haj El Tahir et al.

Title Page

Abstract

Introduction

Conclusions

References

Tables

Figures

◀

▶

◀

▶

Back

Close

Full Screen / Esc

Printer-friendly Version

Interactive Discussion



Soil erosion areas in the Blue Nile-Eastern Sudan

M. El Haj El Tahir et al.

Title Page

Abstract

Introduction

Conclusions

References

Tables

Figures



Back

Close

Full Screen / Esc

Printer-friendly Version

Interactive Discussion



Observed data indicate that the mean annual precipitation in 2006 was 900 mm, of which around 90% is collected during the rainy season (April–October). For erosion we are interested in the inter-annual and not the annual total of rainfall. The maximum two or three rainy days in 2006 are of interest because it is the maximum rainfall that causes erosion. The maximum rainfall occurred on 8 and 10 May with precipitation levels as high as 109.2 mm and 200.6 mm, respectively. The mean annual temperature is 28.8 °C. The lowest daily mean temperature is 13 °C and is measured in December. The highest mean daily temperature is 43.8 °C and is measured in May. The runoff coefficient is 20–30% (Ahmed et al., 2006). The year 2006 was an exceptionally wet year. The normal mean annual rainfall is 500 mm (Abdulkarim, 2006).

Economic impacts of gully erosion in the study region

Although erosion in the centre of the gully is visually apparent (Fig. 2), its effects are not always detectable in terms of changes in soil quality (Ward et al., 2001). This indicates how geomorphologically-apparent desertification (Nir and Klein, 1974; Rozin and Schick, 1996) and changes in soil nutrient content are not necessarily congruent. Nonetheless, a decline in soil nutrients was recorded in some of the most important soil variables, and thus is likely to significantly impact plant growth. Although the major erosion is usually in the centre of the gully in a strip that is only 5–30 m wide, most plant biomass and species diversity is as well concentrated there (Ward and Olsvig-Whittaker, 1993). Moreover, the concentration of the water current in the central erosion gully necessarily reduces the water flow to the adjoining sides of the valley during floods. As a consequence of this reduction in water availability, leaching of salts is reduced (Shalhevet and Bernstein, 1968; Dan et al., 1973; Dan and Yaalon, 1982; Dan and Koyumdjisky, 1987) and soil salinity increases on the sides of the valley. Thus, even in the soil that remains un-eroded, soil quality declines over time.

2.2 Data selection and processing

Nowadays there is a vast reservoir of remote sensing data, some freely available and easily downloadable from the internet. Remote sensing data are described in terms of spatial resolution, temporal resolution, timing, section of the electromagnetic spectrum, stereo, interferometric or ranging capability, and usability (Kääb et al., 2005c). Two types of satellite images are used in this study: Advanced Spaceborne Thermal Emission and Reflection Radiometer (ASTER) and Moderate Resolution Imaging Spectroradiometer (MODIS). In addition, a digital elevation model (DEM) provided by Shuttle Radar Topography Mission (SRTM) was used. Table 1 summarises the data characteristics. The softwares used are PCI Geomatica version 10.1 and ArcGIS version 9.3.

2.2.1 ASTER Data

ASTER is a medium-resolution multispectral satellite sensor on the National Aeronautics and Space Administration (NASA) Terra spacecraft, incorporating also an along-track stereo sensor. The latter has stereo angle of about 28° directed backwards. ASTER has 3 NADIR cameras with bands 1–3 in the visible and near infrared (VNIR), bands 4–9 in the short-wave infrared (SWIR), bands 10–14 in the thermal infrared (TIR). It also has a back-looking stereo camera (band 3B). The five ASTER thermal infrared bands (TIR), i.e. B10–B14, are not used in this study. The nadir channel 3N and the back-looking channel 3B are used to generate photogrammetric DEMs. The time difference between the nadir and the back-looking acquisition is about 1 min (Toutin, 2001c). Moreover, the reasonable image swath of 60 km allows gully identification over wide regions. The raw data is retrieved in HDF (hierarchical data format) formats. It contains image data, ancillary data (date, time, orbits, positions, angles, sensor and satellite settings, etc.), and meta-data. Terra is preferred to Aqua because it registers images during the day. Here, we used ASTER level 1B data with striping removed. The two ASTER images are from 30 March 2006 and 18 December 2006. March on the

Soil erosion areas in the Blue Nile-Eastern Sudan

M. El Haj El Tahir et al.

Title Page

Abstract

Introduction

Conclusions

References

Tables

Figures

◀

▶

◀

▶

Back

Close

Full Screen / Esc

Printer-friendly Version

Interactive Discussion



one hand marks the end of the dry season. The rainy season usually begins in early April. December on the other hand is characterised by high soil moisture conditions since it is just towards the very end of the rainy season. It is also characterised by vigorous seasonal and permanent vegetation growth. The scenes were selected for dates with no cloud cover.

2.2.2 MODIS Data

At a continental or global scale, coarse spatial resolution data such as from MODIS are preferable because they cover much larger spatial scales simultaneously. A combination of multi-sensor data with various image characteristics is usually beneficial to the research (Lefsky and Cohen, 2003). MODIS Terra 13Q data version v005, level 2B (available from http://lpdaac.usgs.gov/faq_ecsftp.asp), is used. Two MODIS images dating to 22 March 2006 and 19 December 2006 are used. The first image is a 16-days average of daily images between the period 14 to 30 March 2006 and the second is a 16-days average of daily images between the periods 2 to 18 December 2006. MODIS products of versions 4 or higher have been validated and approved for scientific research. Each image has 11 data layers originally. Of these 11 layers, only 6 data layers are used. The layers used are: 1, 2, 5, 6, 7, and 8 which correspond to Normalised Difference Vegetation index (NDVI), Enhanced vegetation index (EVI), red reflectance, Near infra red (NIR) reflectance, blue reflectance and medium infra red (MIR) reflectance, respectively.

MODIS vegetation indices (VIs) are found to be sensitive to seasonal vegetation variations, land cover variations, and biophysical parameter variations. Both the NDVI and EVI demonstrate a good dynamic range and sensitivity for monitoring and assessing spatial and temporal variations in vegetation amount and condition (Huete et al., 2002).

Whereas the NDVI is chlorophyll sensitive, the EVI is more responsive to canopy structural variations, including leaf area index (LAI), canopy type, plant physiognomy, and canopy architecture (Gao et al., 2000). The two VIs complement each other in

Soil erosion areas in the Blue Nile-Eastern Sudan

M. El Haj El Tahir et al.

Title Page

Abstract

Introduction

Conclusions

References

Tables

Figures

◀

▶

◀

▶

Back

Close

Full Screen / Esc

Printer-friendly Version

Interactive Discussion



global vegetation studies and improve upon the detection of vegetation changes.

$$NDVI = \frac{(\rho_{NIR} - \rho_{red})}{(\rho_{NIR} + \rho_{red})}$$

Where: ρ_{NIR} and ρ_{red} are the surface bidirectional reflectance factors for their respective MODIS bands. NDVI is successful as a vegetation measure in that it is sufficiently stable to permit meaningful comparisons of seasonal and inter-annual changes in vegetation growth and activity. The strength of the NDVI is in its rationing concept, which reduces many forms of multiplicative noise (illumination differences, cloud shadows, atmospheric attenuation, and certain topographic variations) present in multiple bands.

The Enhanced Vegetation Index (EVI) is a slight derivation from NDVI as it includes one additional spectral band, but no other peripheral data. EVI is designed to improve on NDVI by addressing the weaknesses in NDVI attributed to backscatter and saturation.

$$EVI = \frac{G(\rho_{NIR} - \rho_{red})}{\{\rho_{NIR} + C1\rho_{red}\} - \{C2\rho_{blue} + L\}}$$

Where: G is a gain factor. L is the canopy background adjustment, and $C1$, $C2$ are the coefficients of the aerosol resistance term, which uses the blue band to correct for aerosol influences in the red band.

2.2.3 SRTM Data

Shuttle Radar Topography Mission (SRTM) is a single-pass InSAR, it provides elevation data on a near-global scale (between 60° N and 54° S), it is the most complete high-resolution digital topographic database of Earth, date February 2000, 90 m resolution and 10–20 m vertical accuracy. It has gaps in it that resulted from shadow, SRTM3 is freely available. Where available, the SRTM indeed represents a revolutionary data set for all kinds of terrain studies, in particular also for high-mountain hazard assessments (Kääb et al., 2005c). However, due to radar shadow, foreshortening, lay-over and insufficient interferometric coherence, the SRTM DTM has significant voids

Soil erosion areas in the Blue Nile-Eastern Sudan

M. El Haj El Tahir et al.

Title Page

Abstract

Introduction

Conclusions

References

Tables

Figures

◀

▶

◀

▶

Back

Close

Full Screen / Esc

Printer-friendly Version

Interactive Discussion



in high mountains. In such cases, the fusion between spaceborne photogrammetric DTMs and the SRTM DTM is regarded as a promising approach.

3 Methodology

3.1 Method overview

5 Common erosion mapping techniques integrate products derived from satellite remote sensing with additional data sources. These techniques include quantitative erosion models (e.g., Thornes, 1985; Zhang et al., 2002; Symeonakis and Drake, 2004) and qualitative methods (e.g., Liu et al., 2000, 2004; Vrieling et al., 2002, 2007). The drawbacks of quantitative erosion models include among others fixed and intensive data
10 requirement (Vrieling, 2006). Therefore, a more general qualitative erosion mapping approach is used here based on adaptations to the regional characteristics of the study area and the availability of data. This approach is derived from fusion between remote sensing data and geographical information systems (GIS). GIS has proved to be a particularly useful tool where topographic information (e.g. DEMs and their derivatives) has
15 to be combined with remotely sensed image data and in change detection applications, in particular when multi-source data are used. The flow diagram in Fig. 3 summaries the method used in developing this qualitative erosion area model. Briefly speaking, the study area (Fig. 1) is divided into two scales. One is a 60×60 km scale (approx. 3600 km²) and studied using two different ASTER images from March and December 2006. The other is a 180×180 km regional scale (approx. 32 400 km²) and studied
20 using MODIS data. The ASTER images are first accurately orthorectified using SRTM DEM before being used for classification. The accuracy of SRTM DEM is first compared to two other DEMs, which are extracted from the ASTER scenes themselves. The purpose of the classification is to detect the changes in eroded areas between the two scenes. As such the erosion area between the period March and December
25 2006 is determined at this scale. Using the same training areas from ASTER, two

Soil erosion areas in the Blue Nile-Eastern Sudan

M. El Haj El Tahir et al.

Title Page

Abstract

Introduction

Conclusions

References

Tables

Figures

◀

▶

◀

▶

Back

Close

Full Screen / Esc

Printer-friendly Version

Interactive Discussion



georeferenced MODIS senses from the same period i.e. March and December 2006 are classified. The change in eroded area on this larger scale is hence determined. In this model we generalised the results of studying smaller area of approx. 3600 km² to larger area of approx. 32 400 km². This is achieved by working out a fusion between remote sensing and GIS.

3.2 ASTER DEM generation and orthorectification

Accurate geometric rectification or image registration of remotely sensed data is a prerequisite for combining different source data in a classification process (Jensen, 1996; Lu et al., 2004; Toutin, 2004; Kääb et al., 2005b; Lu and Weng, 2007). In particular orthoprojection of high and medium resolution satellite and aerial image data is a mandatory pre-processing step, necessary to prevent strong topographically induced distortions between the images in rugged or mountainous regions (Kääb, 2005a). Accordingly, with an elevation range between approximately 10 m and 1500 m in the study area the ASTER scenes used had to be orthorectified. For this purpose, two DEMs are extracted from the two ASTER images in addition to the SRTM DEM. The three DEMs are then compared (Figs. 4a–5) and the most accurate of the three is found to be SRTM DEM which is eventually used to orthorectify the ASTER images.

DEM generation from satellite imagery uses photogrammetric principles. (Toutin, 2001a, 2002b; Toutin and Cheng, 2001, 2002) outlined the main digital processing steps for DEM generation from ASTER within the PCI Geomatica software. The principle of the binocular disparity (or parallax) is applied in satellite photogrammetry to compute the terrain elevation from the measured parallaxes between the two images (Toutin, 2001). Modern stereoscopy uses images to produce a three dimensional (3-D) visual model with characteristics analogous to that of actual features viewed using true binocular vision. Photogrammetric principles for space photos (collinearity and coplanarity conditions) and their equivalent for remote sensing data mathematically solve the relationship between two dimensional (2-D) image co-ordinates and 3-D ground co-ordinates. Eventually when two or more images overlap then DEM can be computed.

Soil erosion areas in the Blue Nile-Eastern Sudan

M. El Haj El Tahir et al.

Title Page

Abstract

Introduction

Conclusions

References

Tables

Figures

◀

▶

◀

▶

Back

Close

Full Screen / Esc

Printer-friendly Version

Interactive Discussion



Sterephogrammetry constructs a ray in space to a specific pixel. The intersection is the real three dimensional measurement of the point in the ground. It is possible to measure both vertical and horizontal displacements. All unknown variables are solved for using a least-square bundle adjustment. From this, epipolar images are created from the 3N and 3B bands and height parallaxes matched using cross-correlation techniques. The 3-D stereo model parameters are then applied to transform the raw DEM to cartographic ground coordinates. Sterephogrammetry has the advantage that the correlation coefficients obtained during the parallax matching process give an idea of how accurate is the computed DEM (known in PCI Geomatica as the score channel). ASTER stereo has one minute difference between the two cameras the NADIR looking and the back looking giving simultaneous along-track stereo-data acquisition a strong advantage in terms of radiometric variations. Larger time intervals are undesirable because there would be changes in the area where the image was acquired. Stereo photogrammetry is a well-developed practice with high correlation success rates.

The first three channels (NADIR) 123N and the back looking channel 3B of ASTER 30 March 2006 are read as two different .pix files in PCI Geomatica's orthoengine using Toutin's low resolution model. The scenes are reprojected to UTM WGS1984 Zone 36N projection. The ground control points (GCPs) necessary for estimating the model parameters are collected from a hillshade image of SRTM generated in ArcGIS.

In total 29 GCPs are collected. The Root Mean Square Error (RMS) is 0.98 pixels (13.28 m). The two images 123N and 3B were tied together using 95 tie points. The maximum residual for tie points is 0.77 pixels (8.67 m). Using cubic transformation and SRTM DTM as the Dem source, a 60 m resolution DEM is extracted. The same procedure is repeated using the second ASTER image of 18 December 2006. A second 60 m resolution DEM is extracted using 31 GCPs, and the Root Mean Square Error (RMS) obtained is 1.08 pixels (14.63 m) (Table 2).

The reason for using the hillshade of SRTM for collecting GCPS is due to the lack of accurate topographic maps for the study area. The hillshade SRTM ensures better co-registration between the SRTM DEM and the ASTER-derived products later in the

Soil erosion areas in the Blue Nile-Eastern Sudan

M. El Haj El Tahir et al.

Title Page

Abstract

Introduction

Conclusions

References

Tables

Figures



Back

Close

Full Screen / Esc

Printer-friendly Version

Interactive Discussion



combination process between the two.

3.3 Comparison of the three DEMs

Because the two generated ASTER DTMs cannot be tested against existing reference DTMs, they are tested through the overlay of orthoimages, generated from imagery from different sensor positions (multi-incidence angle images). The horizontal projection shifts between the orthoimages from different source imagery is visualized by the following:

- ratio images, (change detection techniques)
- image flickering (animation techniques)

Due to radar shadow, foreshortening, layover and insufficient interferometric coherence, the SRTM DTM has significant voids in high mountains topography, but show considerably smaller gross errors compared to ASTER-derived DTMs (Kääb, 2005a).

Visual inspection and quantitative analysis show that severe vertical errors of the ASTER DTM of up to 500m occur for sharp peaks having steep northern slopes. These errors are not surprising, considering that northern slopes are heavily distorted (or even totally hidden) in the 27.6° back-looking band 3B, and lie in shadow at the same time. The two ASTER DTMs were generated from level 1A ASTER images for 6 March and 18 December 2006 and projected to WGS 1984 UTM Zone 36N. The accuracy obtained for the ASTER DTMs compared to the SRTM amounts to ± 78 m RMS (for 6 March 2006) and ± 68 m RMS (18 December 2006). Maximum errors range between -220 m and $+500$ m. The vertical differences between the 6 March and 18 December 2006-derived DTMs amount to ± 33 m RMS (range: -380 m to $+180$ m). For a subsection with moderate high-mountain topography, an accuracy of ± 15 m RMS (for the 6 March DTM: ± 19 m) and maximum errors of 100 m were found (for the 18 December DTM: 105 m). For the subset, the vertical differences between the 6 March and 18 December-derived DTMs lie in the range of ± 11 m RMS, with maximum errors

Soil erosion areas in the Blue Nile-Eastern Sudan

M. El Haj El Tahir et al.

Title Page

Abstract

Introduction

Conclusions

References

Tables

Figures

◀

▶

◀

▶

Back

Close

Full Screen / Esc

Printer-friendly Version

Interactive Discussion



Soil erosion areas in the Blue Nile-Eastern Sudan

M. El Haj El Tahir et al.

| | |
|--------------------------|--------------|
| Title Page | |
| Abstract | Introduction |
| Conclusions | References |
| Tables | Figures |
| ◀ | ▶ |
| ◀ | ▶ |
| Back | Close |
| Full Screen / Esc | |
| Printer-friendly Version | |
| Interactive Discussion | |

between -30 m and +50 m. These maximum errors occur at sharp ridges or deep gullies. Generally speaking the accuracy of GCPs and the radiometric image contrast are among the main factors limiting the accuracy of the extracted DEM (Toutin, 2001b, 2002a; Toutin and Cheng, 2001). In this case the low accuracy of the ASTER DEM is attributed to the low optical contrast of the study area. When plotted, the score channel showed that the highest values of over 90% around the lake (Fig. 6). When compared to the SRTM DEM, the ASTER DEM showed differences of up to 650–750 m (Figs. 4a–5). Compared to the SRTM DEM, the ASTER DEM overestimates elevation at higher latitudes while it underestimates elevation at low altitudes. Accordingly SRTM was used to orthoproject the two ASTER images.

The depicted test area represents rugged high-mountain conditions with elevations of up to 1500 m a.s.l., steep rock walls, deep shadows that are without contrast. Therefore, the test area is considered to represent a worst case for DTM generation from ASTER data.

3.4 ASTER classification

For the purpose of classification only orthoprojected ASTER VNIR channels (1, 2, and 3) and SWIR channels (4, 5, 6, 7, 8, and 9) are used. ASTER thermal channels (10–15) and back-looking channels (3B) were not used.

Slope and aspect are important geomorphic parameters. Slope measures the rate of change of elevation in the direction of the steepest descent (Gallant and Wilson, 2000). It is the means by which gravity induces flow of water and other materials, therefore it is of great importance in geomorphology. The aspect of a slope controls its solar irradiation, thus affecting a wide diversity of processes (Moore et al., 1991). Slope and aspect can be calculated from a digital elevation model using one of several GIS-based algorithms (e.g., Moore et al., 1991; Burrough and McDonnell, 1998). ArcGIS uses a type of Finite difference method that uses eight neighbours to calculate aspect and slope. The slope and aspect are calculated from the SRTM elevation data. They are then resampled to 15 m in order to stack them as two additional layers to the



orthprojected ASTER image layers.

Additionally, the river flow network was estimated using the hydrologic analysis package in ArcGIS 9.2. When working with raster DEMs and computing slopes between grid cells, the ratio of the vertical and horizontal resolutions determines the minimum non-zero slope that can be resolved. In this study, the vertical resolution of the DEM is 1 m and a grid size is 15 m. Therefore the resolvable slope of $1/15=0.0667$. This value means that slopes on hillsides can be computed with a relatively small error. However, slopes in channels are often much smaller than this value. As a consequence, these areas will appear horizontal in the DEM and require special techniques for flow routing in horizontal areas. The technique suggested below is thought to produce consistent results in areas where the flow of water is governed by features that are smaller than the resolution or uncertainty of the DEM, in this case 15 m.

This technique of deriving flow direction from a digital elevation model (DEM) is presented in Jenson and Domingue (1988) and is used in ArcGIS 9.2 Network Analyst function. The direction of flow is determined by finding the direction of steepest descent, or maximum drop, from each cell. This is calculated as

maximum drop = change in z -value/distance

The distance is calculated between cell centres. This approach is commonly referred to as an eight direction (D8) flow model since there are eight valid output directions relating to the eight adjacent cells into which flow could travel.

One challenge arises if all neighbours are higher than the processing cell. In such case the processing cell is called a sink and has an undefined flow direction because any water that flows into a sink cannot flow out. To obtain an accurate representation of flow direction across a surface, the sinks should be filled. The minimum elevation value surrounding the sink will identify the height necessary to fill the sink so the water can pass through the cell. A digital elevation model (DEM) free of sinks is called depressionless DEM. When handling sinks it is important to understand the morphology of the area well so as to be able to distinguish features that may truly be sinks on the

Soil erosion areas in the Blue Nile-Eastern Sudan

M. El Haj El Tahir et al.

Title Page

Abstract

Introduction

Conclusions

References

Tables

Figures

◀

▶

◀

▶

Back

Close

Full Screen / Esc

Printer-friendly Version

Interactive Discussion



surface of the earth from others which are merely errors in the data or NoData values. Using the depressionless DEM as an input to the flow direction process, the direction in which water would flow out of each cell is determined.

The flow accumulation, also known as contributing area determines the size of the region over which water from rainfall can be aggregated. As specific catchment area and slope steepness increase, the amount of water contributed by upslope areas and the velocity of water flow increase, hence stream power and potential erosion increase (Moore et al., 1988). Therefore flow accumulation is very important in describing flow erosion. In flow accumulation, the initial stage is defining the stream network system. Thereafter an appropriate threshold value is determined for stream network delineation. A stream network is created by applying a threshold value to select cells with a high accumulated flow. A break in slope can often be identified in a scatter plot of slope versus area as explained by Tarboton et al. (1991) to identify this threshold.

The final ASTER orthoimages used for classification consisted of 13 layers stacked together. These include: VNIR channels 1, 2, and 3, SWIR channels 4, 5, 6, 7, 8, and 9, SRTM DEM, slope, aspect, and river flow network.

For supervised classification, the image was trained into four land cover types: Gully, Mountain, Flat_land, and Water. NoData were allowed as additional classification output. The most challenging task is to separate between Flat_land and Gullies since these two classes are bound to overlap. Overlapping training area boundaries reduces the reliability of the training sites. To achieve this goal, firstly the layer of river network is superimposed on top of the image to help guide to discriminate between gullies and flat lands. Secondly reliance is made of the author's knowledge of the area and with the aid of a selection of digital photographs taken during an eight weeks field trip in 2006/2007. Thirdly care is taken when selecting the different bands both for display, in either greyscale or as colour composites in the Focus viewer, for training area digitizing, and for the classification algorithm. According to Asner and Heidebrecht (2002) ASTER's SWIR (2.0–2.3 μm) i.e. bands 6, 7, 8, and 9 spectral region is one of the best ways to estimate the fractional cover of photosynthetic vegetation, non-photosynthetic

Soil erosion areas in the Blue Nile-Eastern Sudan

M. El Haj El Tahir et al.

Title Page

Abstract

Introduction

Conclusions

References

Tables

Figures

◀

▶

◀

▶

Back

Close

Full Screen / Esc

Printer-friendly Version

Interactive Discussion



vegetation, and bare soils in arid regions. The VNIR channels are important for discriminating vegetation and water, whereas SWIR are important for discriminating bare soil. As many training areas as possible are trained because generally speaking, the more areas identified as training sites, the higher the accuracy of the classification.

5 Once the training areas are defined, then the signature separability values are studied. Signature separability is the statistical difference between pairs of spectral signatures. It is expressed in terms of Bhattacharyya Distance and Transformed Divergence. These are measures of the separability of a pair of probability distributions. Both Bhattacharyya Distance and Transformed Divergence are shown as real values between
10 zero and two. Zero indicates complete overlap between the signatures of two classes, two indicates a complete separation between the two classes. The higher the separability (i.e. more than 1.5) value the more accurate is the classification accuracy.

Eventually supervised classification is run several times and the accuracy reports from each run are compared. The accuracy report showed values for average and
15 overall accuracies and kappa coefficient (Table 3). Between each run the classes are refined, the numbers of training areas are varied, and different band combinations are tried, until better accuracies are achieved.

After running the first successful classification, the signature statistic report is studied in order to understand which channels mostly contributed to gully identification. Lu and Weng (2007) advice that it is important to select only the variables that are most
20 useful for separating land-cover or vegetation classes, especially when hyperspectral or multisource data are employed. The results showed that aspect shows high standard deviation values and hence it is the least significant in delineating gullies (Fig. 7). By contrast slope and river network had the least standard deviation and hence they
25 are more important in identifying gullies. Short-wave infrared channels have less standard deviation than visible and near infra red bands. Slope contributed more to gully classification accuracy than the actual elevation.

Therefore, aspect and elevation layers were finally removed from the image layer stack. Classification was re-run again producing better accuracies.

Soil erosion areas in the Blue Nile-Eastern Sudan

M. El Haj El Tahir et al.

Title Page

Abstract

Introduction

Conclusions

References

Tables

Figures



Back

Close

Full Screen / Esc

Printer-friendly Version

Interactive Discussion



Next, an accuracy assessment was designed and implemented. A random sample of 300 points was generated in PCI Geomatica and compared to the original ASTER image. ASTER image is used as a reference image due to lack of accurate and updated maps for the study area. Each of the 300 samples was checked and assigned to the different classes. Table 4 summarise the outcome of the accuracy assessment.

The two classified images of March and December 2006 are laid on top of each other and the area where they overlap is selected to study the bi-temporal change (Fig. 8).

3.5 MODIS classification

First MODIS products of 22 March 2006 are classified in order to generalise the results of the ASTER classification to larger area covering the whole of the Blue Nile province. As mentioned earlier MODIS constituted of a 16-days average of daily images between the periods 14 to 30 March 2006 with 11 data layers originally, of which only 6 i.e. NDVI, EVI, red reflectance, NIR reflectance, blue reflectance and MIR reflectance data layers are used. MODIS is first re-projected to UTM WGS1984 Zone 36N. Thereafter, the same training areas from ASTER 30 March 2006 are used to run a supervised maximum likelihood classifier. The four land cover types are Gully, Mountain, Flat Land, and Water. The classification accuracies are shown in Table 5.

Accuracy assessment is run via generating random samples in PCI Geomatica and using the original 6 March ASTER as reference image. The results are shown in Table 6.

Further check is performed using a set of thirteen digital photos with registered coordinates taken in January 2007 from different locations. Nine of the photos showed similar land cover types as in the classified image. The same procedure is repeated for the MODIS products of 19 December 2006.

Soil erosion areas in the Blue Nile-Eastern Sudan

M. El Haj El Tahir et al.

Title Page

Abstract

Introduction

Conclusions

References

Tables

Figures

◀

▶

◀

▶

Back

Close

Full Screen / Esc

Printer-friendly Version

Interactive Discussion



4 Results and discussion

The two ASTER classified images from March and December 2006 are overlaid and their overlap area is extracted. For each image the area represented by each land cover type is calculated using the function Generate Area Report in PCI Geomatica. The results are shown in Table 7. The areas in the December image are subsequently subtracted from their correspondent in the March image in order to calculate the changed area per each land cover type. i.e. the area of each land cover type is calculated for both dates and the difference between the two gives an estimate of the bi-temporal change. Ultimately a bi-temporal change map is produced (Fig. 8). Table 7 shows an increase by approx. 112 km^2 in the area of gullies. This is because after the rainy season, both rain and flood water dissects large areas creating either new gullies or increasing the width and/or depth of existing gullies. Naturally an increase in dissected land reduces the extent of flat land. That is why there is a decrease of flat land by 153 km^2 . The area covered with water has increased by 31.5 km^2 . That is due to the fact that in December there were still large areas that are covered with rain and flood water from the rainy season time which have not receded, percolated or evaporated yet. That is particularly true for areas around Ar Roseris Dam Lake. The total area classified as mountains did not change. In fact this is regarded as an indication of the success of the classification because Kääb, (2005a) argues that an important indication of either good georeferencing or subsequently good multitemporal analysis is the fact that stable features like mountains remain stable.

The bi temporal change is viewed in connection with the classification accuracies of the two images and the pixel size of ASTER to see how significant these results are. The classified images of March and December have average classification accuracies of 93.37% and 86.79%, respectively. Therefore their statistical error is approximately 6.63% and 13.21%, respectively. As for the pixel size, it must also be noted that the spatial width of the seasonal gullies which are the main focus of the study is very variable (between 2 m to 20 m or more). The maximum image resolution of 15 m could

Soil erosion areas in the Blue Nile-Eastern Sudan

M. El Haj El Tahir et al.

Title Page

Abstract

Introduction

Conclusions

References

Tables

Figures

◀

▶

◀

▶

Back

Close

Full Screen / Esc

Printer-friendly Version

Interactive Discussion



lead to overlooking of gullies that are too small or too big.

Similar to area estimations using ASTER, the changes in the different land cover areas are estimated from the two classified MODIS products. Table 8 shows that gullies and water have increased by approx. 2071 and 1791 km², respectively, flat land has decreased by 3864 km² while mountains remained unchanged. MODIS classification accuracy around 80% in an area that is predominantly rural with few land cover/use classes is good. There is insufficient spectral distinctiveness due to the low spectral and spatial resolution of the MODIS data. The training classes were based on ASTER data that has higher spatial and spectral resolution causing some discrepancies between the two data sets. MODIS products consisted of averaged products rather than the actual spectral bands. Some artefacts interfered with the calculation of eroded area.

Hence the estimated area along the Blue Nile River, between Sennar and Ed Damazin, Eastern Sudan that was affected by soil erosion during the 2006 rainy season was estimated to be 2071 km² or 6.5% of the total study area approximately. This estimation should be viewed in light of the facts that: a) the year 2006 was exceptionally wet year compared to previous years, b) the Upper Blue Nile River is steeper and receives more rain than any other river in Sudan namely, the White Nile, River Atbara, Sobat, etc, c) there are no previous studies on areas affected by seasonal erosion on this particular region to compare these results with.

5 Conclusions

An understanding of soil erosion is mandatory for any consequent understanding of soil moisture regime in Blue Nile region, Eastern Sudan. On its own rights, soil erosion poses a serious environmental and socio-economic threat to the environment and mankind. Previous research in Sub-Sahara Africa has singled out the Upper Blue Nile as an erosion prone area that is recommended for further monitoring and evaluation.

In this study a qualitative soil erosion area model was suggested. The model bene-

Soil erosion areas in the Blue Nile-Eastern Sudan

M. El Haj El Tahir et al.

Title Page

Abstract

Introduction

Conclusions

References

Tables

Figures

◀

▶

◀

▶

Back

Close

Full Screen / Esc

Printer-friendly Version

Interactive Discussion



fits from advances in GIS and remote sensing fusion techniques. The model is simple, robust and straightforward. It makes use of the well tested methods of supervised classification using maximum likelihood (MLC). Generalisation of ASTER classification results using MODIS was useful for capturing a regional impression of the spatial distribution of erosion. Key to the model success is further development of proper validation procedures. The model can be used to study longer-term changes in erosion by using a images from different years.

The size of this region makes the traditional mapping methods of aerial photography and field surveying of limited use. Moderate resolution multispectral data allows continental- to global-scale mapping of the Earth's surface while retaining sufficient resolution for geomorphic and ecological studies.

The methodology presented here is also transportable to other arid and semi-arid parts of Sudan where an understanding of soil erosion is desirable.

Acknowledgements. Our appreciation extends to the Norwegian Research Council (NFR) for sponsoring the project number 171783 (FRIMUF), Department of Geosciences, University of Oslo, Faculty of Engineering, University of Khartoum, The Forestry, Irrigation and Environment National Corporations of the Sudan.

References

- Abdulkarim, A.: Rainfall Variability in the Blue Nile State, Reports of the National Meteorological Office, Khartoum, 2006.
- Ahmed, A., Osman Ishraga, S., and Babiker, A.: Sediment and Aquatic Weeds Management Challenges in Gezira Irrigated Scheme. Proceedings, UNESCO's International Sediment Initiative Conference (ISIC), Khartoum, Sudan, 2006.
- Asner, G. P. and Heidebrecht, K. B.: Spectral unmixing of vegetation, soil and dry carbon cover in arid regions: comparing multispectral and hyperspectral observations, *Int. J. Remote. Sens.*, 23(19), 3939–3958, 2002.
- Ayoub A. T.: Extent, severity and causative factors of land degradation in the Sudan, *J. Arid Environ.*, 38, 397–409, 1998.

Soil erosion areas in the Blue Nile-Eastern Sudan

M. El Haj El Tahir et al.

Title Page

Abstract

Introduction

Conclusions

References

Tables

Figures

◀

▶

◀

▶

Back

Close

Full Screen / Esc

Printer-friendly Version

Interactive Discussion



Soil erosion areas in the Blue Nile-Eastern Sudan

M. El Haj El Tahir et al.

Title Page

Abstract

Introduction

Conclusions

References

Tables

Figures

◀

▶

◀

▶

Back

Close

Full Screen / Esc

Printer-friendly Version

Interactive Discussion



Bull, W. B.: Soils, geology, and hydrology of deserts, in: *Water in Desert Ecosystems*, edited by: Evans, D. D. and Thames, J. L., 42–58, Dowden, Hutchinson and Ross, Stroudsburg, PA, 280 pp., 1981.

Burrough, P. A. and McDonald, R. A.: *Principles of Geographical Information Systems*, Oxford University Press, New York, 333 pp., 1998.

Crawford, C. S. and Gosz, J. R.: *Desert ecosystems: their resources in space and time*, *Environ. Conserv.*, 9, 181–195, 1982.

Dan, J., Moshe, R., and Alperovitch, N.: The soils of Sede Zin, *Israel J. Earth Sci.*, 22, 211–227, 1973.

Dan, J. and Yaalon, D. H.: Automorphic saline soils in Israel, in: *Aridic Soils and Geomorphic Processes*, edited by: Yaalon, D. H., *Cathena Supplement 1*, Cathena Verlag, Braunschweig, Germany, 103–115, 1982.

Dan, J. and Koyumdjisky, H.: Distribution of salinity in the soils of Israel, *Israel J. Earth Sci.*, 36, 213–223, 1987.

Evenari, M., Shanan, L., and Tadmor, N.: *The Negev: The Challenge of a Desert*, Harvard University Press, Cambridge, Mass, 437 pp., 1982.

Fadul, H. M., Salih, A. A., Ali, A., and Inanga, S.: Use of remote sensing to map gully erosion along Atbara River, Sudan, *JAG*, 1(3/4), 1999.

Fadul, H. M.: Use of Remote Sensing in Monitoring Impacts of Bank and Back Gully Erosion in Sudan, *Proceedings, UNESCO's International Sediment Initiative Conference (ISIC)*, Khartoum, Sudan, 2006.

Gao, X., Huete, A., Ni, W., and Miura T.: Optical–biophysical relationships of vegetation spectra without background contamination, *Remote Sens. Environ.*, 74, 609–620, 2000.

Gallant, J. C. and Wilson, J. P.: Primary topographic attributes, in: *Terrain Analysis: Principles and Applications*, edited by: Wilson, J. P. and Gallant, J. C., John Wiley and Sons, Inc., New York, 51–85, 2000.

Gomer, D. and Vogt, T.: Physically based modelling of surface runoff and soil erosion under semi-arid Mediterranean conditions, the example of Oued Mina, Algeria, in: *Soil Erosion: Application of Physically Based Models*, edited by: Schmidt, J., Springer Verlag, Berlin, Heidelberg, New York, 58–78, 2000.

Gruber, S. and Peckham, S.: Land-surface parameters and objects in hydrology, *Dev. Soil Sci.*, 33, 171–194, 2009.

Huete, A., Didan, K., Miura, T., and Rodriguez, E.: Overview of the radiometric and biophysical

performance of the MODIS vegetation indices, *Remote Sens. Environ.*, 83(1–2), 195–213, 2002.

Jensen, J. R.: *Introductory Digital Image Processing: A Remote Sensing Perspective*, Prentice-Hall, Englewood Cliffs, NJ, 379 pp., 1996.

5 Jensen, S. K. and Domingue, J. O.: Extracting topographic structure from digital elevation data for geographic information system analysis, *Photogramm. Eng. Rem. S.*, 54(11), 1593–1600, 1988.

Kääb, A.: Combination of SRTM3 and repeat ASTER data for deriving alpine glacier flow velocities in the Bhutan Himalaya, *Remote Sens. Environ.*, 94(4), 463–474, 2005a.

10 Kääb, A.: *Remote Sensing of Mountain Glaciers and Permafrost Creep*, Schriftenreihe Physische Geographie, vol. 48, Geographisches Institut der Universität Zürich, Zürich, Switzerland, 266 pp., 2005b.

Kääb, A., Huggel, C., Fischer, L., Guex, S., Paul, F., Roer, I., Salzmann, N., Schlaefli, S., Schmutz, K., Schneider, D., Strozzi, T., and Weidmann, Y.: Remote sensing of glacier- and permafrost-related hazards in high mountains: an overview, *Nat. Hazards Earth Syst. Sci.*, 5, 527–554, 2005,

<http://www.nat-hazards-earth-syst-sci.net/5/527/2005/>.

Lefsky, M. A. and Cohen, W. B.: Selection of remotely sensed data, in: *Methods and Applications for Remote Sensing: Concepts and Case Studies*, edited by: Wulder, M. A. and Franklin, S. A., Kluwer Academic Publishers, Dordrecht, 13–46, 2003.

20 Linsley Jr., R. K., Kohler, M. A., and Paulhus, J. L. H.: *Hydrology for Engineers*, 3rd edition, International Student Edition, McGraw-Hill Kogakusha, Ltd., New York, USA, 1982.

Liu, J. G., Hilton, F., Mason, P., and Lee, H.: A RS/GIS study of rapid erosion in SE Spain using ERS SAR multi-temporal interferometric coherence imagery, in: *Remote Sensing for Agriculture, Ecosystems, and Hydrology II*, edited by: Owe, M., Zilioli, E., and D’Urso, G., Proceedings of SPIE, vol. 4171, SPIE International, Barcelona, Spain, 367–375, 2000.

25 Liu, J. G., Mason, P., Hilton, F., and Lee, H.: Detection of rapid erosion in SE Spain: A GIS approach based on ERS SAR coherence imagery, *Photogramm. Eng. Rem. S.*, 70(10), 1179–1185, 2004.

30 Lu, D., Mausel, P., Brondizio, E., and Moran, E.: Change detection techniques, *Int. J. Remote Sens.*, 25(12), 2365–2407, 2004.

Lu, D. and Weng, Q.: A survey of image classification methods and techniques for improving classification performance, *Int. J. Remote Sens.*, 28(5), 823–870, 2007.

Soil erosion areas in the Blue Nile-Eastern Sudan

M. El Haj El Tahir et al.

Title Page

Abstract

Introduction

Conclusions

References

Tables

Figures

◀

▶

◀

▶

Back

Close

Full Screen / Esc

Printer-friendly Version

Interactive Discussion



- Mirghani, O.: Report on the Field Visit to Sennar and Blue Nile States, as part of the December 2006/January 2007 Field work report, Environment National corporation, Khartoum, Sudan, 2007.
- Mokwunye, U.: Nutrient Depletion: Sub-Saharan Africa's Greatest Threat to Economic Development, STAP Expert Workshop on Land Degradation, Dakar, Senegal, 95 pp., 1996.
- Moore, I. D., O'Loughlin, E. M., and Burch, G. J.: A contour-based topographic model for hydrological and ecological applications, *Earth Surf. Proc. Land Forms*, 13(4), 305–320, 1988.
- Moore, I. D., Grayson, R. B., and Ladson, A. R.: Digital terrain modelling: a review of hydrological, geomorphological, and biological applications, *Hydrol. Process.*, 5, 3–30, 1991.
- Nakileza, B., Nsubuga, E. N. B., Tenywa, M. M., and Lwakuba, A.: Rethinking Natural Resource Degradation in Semi-Arid Sub-Saharan Africa: A review of soil and water conservation research and practice in Uganda, with particular emphasis on the semi-arid areas, Overseas Development Institute (ODI) Report, University of Makerere press, Kampala, Uganda, 1999.
- Nearing, M. A., Pruski, F. F., and O'Neal, M. R.: Expected climate change impacts on soil erosion rates, a review. *J. Soil Water Conserv.*, 59(1), 43–50, 2004.
- Nir, D. and Klein, M.: Gully erosion induced in land size in a semi-arid terrain (Nahal Shiqma, Israel), *Z. Geomorphol.*, 21(Suppl.), 191–201, 1974.
- Rozin, U. and Schick, A.: Land use change, conservation measures and stream channel response in the Mediterranean/semiarid transition zone: Nahal Hoga, southern coastal plain, Israel, in: *Erosion and Sediment Yield: Global and Regional Perspectives*, vol. 236, IAHS Press, Centre for Ecology and Hydrology, Wallingford, OX 10 8 BB, UK, 427–443, 1996.
- Schlesinger, W., Reynolds, J. F., Cunningham, G. L., Huenneke, L. F., Jarrell, W. M., Virginia, R. A., and Whitford, W. G.: Biological feedbacks in global desertification, *Science*, 247, 1043–1048, 1990.
- Schlesinger, W., Raikes, J. A., Hartley, A. E., and Cross, A. F.: On the spatial pattern of soil nutrients in desert ecosystems, *Ecology*, 77, 364–374, 1996.
- Shalhevet, J. and Bernstein, L.: Effects of vertically heterogeneous soil salinity on plant growth and water uptake, *Soil Sci.*, 106, 85–93, 1968.
- Symeonakis, E. and Drake, N.: Monitoring desertification and land degradation over sub-Saharan Africa, *Int. J. Remote Sens.*, 25(3), 573–592, 2004.
- Tarboton, D. G., Bras, R. L., and Rodriguez-Iturbe, I.: On the extraction of channel networks from digital elevation data, *Hydrol. Process.*, 5, 81–100, 1991.

Soil erosion areas in the Blue Nile-Eastern Sudan

M. El Haj El Tahir et al.

Title Page

Abstract

Introduction

Conclusions

References

Tables

Figures

◀

▶

◀

▶

Back

Close

Full Screen / Esc

Printer-friendly Version

Interactive Discussion



Thornes, J. B.: The ecology of erosion, *Geography*, 70, 222–234, 1985.

Thornes, J. B.: The interaction of erosional and vegetation dynamics in land degradation: spatial outcomes, in: *Vegetation and Erosion*, edited by: Thornes, J. B., John Wiley, Chichester, 41–53, 1990.

5 Toutin, T.: DEM generation from new VIR Sensors: Ikonos, ASTER and Landsat 7. Proceedings, IGARSS '01, Sydney, Australia, 2001a.

Toutin, T.: Elevation modelling from satellite visible and infrared (VIR) data, *Int. J. Remote Sens.*, 22(6), 1097–1125, 2001b.

Toutin, T. and Cheng, P.: DEM generation with ASTER stereo data, *Earth Observation Magazine*, 10(6), 10–13, 2001.

10 Toutin, T.: DEM from stereo Landsat 7 ETM data over high relief areas, *Int. J. Remote Sens.*, 23(10), 2133–2139, 2002a.

Toutin, T.: Three-dimensional topographic mapping with ASTER stereo data in rugged topography, *IEEE T. Geosci. Remote*, 40(10), 2241–2247, 2002b.

15 Toutin, T. and Cheng, P.: Comparison of automated digital elevation model extraction results using along-track ASTER and across-track SPOT stereo images, *Opt. Eng.*, 41(9), 2102–2106, 2002.

Toutin, T.: Geometric processing of remote sensing images: models, algorithms and methods, *Int. J. Remote Sens.*, 25(10), 1893–1924, 2004.

20 Vrieling, A., Sterk, G., and Beaulieu, N.: Erosion risk mapping, a methodological case study in the Colombian Eastern Plains, *J. Soil Water Conserv.*, 57(3), 158–163, 2002.

Vrieling, A.: Satellite remote sensing for water erosion assessment: a review, *Catena*, 65, 2–18, 2006.

25 Vrieling, A., Rodrigues, S. C., Bartholomeus, H., and Sterk, G.: Automatic identification of erosion gullies with ASTER imagery in the Brazilian Cerrados, *Int. J. Remote Sens.*, 28(12), 2723–2738, 2007.

Ward, D. and Olsvig-Whittaker, L.: Plant species diversity at the junction of two desert biogeographic zones, *Biodivers. Lett.*, 1, 172–185, 1993.

30 Ward, D., Feldman, K., and Avni, Y.: The effects of loess erosion on soil nutrients, plant diversity and plant quality in Negev desert wadis, *J. Arid Environ.*, 48, 461–473, 2001.

West, N. E.: Nutrient cycling in soils of semiarid and arid regions, in: *Semiarid Lands and Deserts: Soil Resource and Rehabilitation*, edited by: Skujins, J., Marcel Dekker, Inc., New York, 648 pp., 295–332, 1991.

Soil erosion areas in the Blue Nile-Eastern Sudan

M. El Haj El Tahir et al.

Title Page

Abstract

Introduction

Conclusions

References

Tables

Figures

◀

▶

◀

▶

Back

Close

Full Screen / Esc

Printer-friendly Version

Interactive Discussion



Xu, C.-Y., Zhang, Q., El Hag El Tahir, M., and Zhang, Z.: Statistical properties of the temperature, relative humidity, and solar radiation in the Blue Nile- Eastern Sudan region. *Theor. Appl. Climatol.*, accepted, online available at: <http://www.springerlink.com/content/47713r157550l230/> 2009.

- 5 Zhang, X., Drake, N., and Wainwright, J.: Scaling land surface parameters for global-scale soil erosion estimation, *Water Resour. Res.*, 38(9), 191–199, 2002.

HESSD

7, 135–177, 2010

**Soil erosion areas in
the Blue Nile-Eastern
Sudan**

M. El Haj El Tahir et al.

Title Page

Abstract

Introduction

Conclusions

References

Tables

Figures

◀

▶

◀

▶

Back

Close

Full Screen / Esc

Printer-friendly Version

Interactive Discussion



Soil erosion areas in the Blue Nile-Eastern Sudan

M. El Haj El Tahir et al.

Table 1. Data description.

| Name | Spatial resolution | Temporal resolution | Swath | Used Bands | Date |
|-------------|--------------------------------------|---------------------|------------|-----------------------------------|-----------------------------|
| ASTER-Terra | 15 m | Daily | 60×60 km | VNIR (1,2,3) and SWIR (5,6,7,8,9) | 30 Mar 2006 and 18 Dec 2006 |
| MODIS-Terra | 500 m | 15-day average | 180×180 km | 1,2,5,6,7,8 | 22 Mar 2006 and 19 Dec 2006 |
| SRTM | 90 m 10–20 m vertical accuracy | | | | 11 Feb 2000 |

Title Page

Abstract

Introduction

Conclusions

References

Tables

Figures

◀

▶

◀

▶

Back

Close

Full Screen / Esc

Printer-friendly Version

Interactive Discussion



Soil erosion areas in the Blue Nile-Eastern Sudan

M. El Haj El Tahir et al.

Table 2. Table: 2 Root mean square error (RMS) for the (GCPs).

| Image | Channel | GCP | RMS | X RMS | Y RMS |
|-------------------|-----------------|-----|--------------------------|-------------------------|-------------------------|
| ASTER 30 Mar 2006 | Nadir 123N | 29 | 0.98 pixels (13.28 m) | 0.81 pixel (12.00 m) | 0.65 pixel (8.01 m) |
| ASTER 30 Mar 2006 | Back-looking 3B | 29 | 1.69 pixels (23.76 m) | 0.87 pixel (11.90 m) | 1.31 pixel (17.26 m) |
| ASTER 18 Dec 2006 | Nadir 123N | 31 | 1.08 pixels (14.63 m) | 0.84 pixel (12.06 m) | 0.67 pixel (8.29 m) |
| ASTER 18 Dec 2006 | Back-looking 3B | 31 | 1.72 pixels (24.19 m) | 0.91 pixel (13.01 m) | 1.47 pixel (20.40 m) |

Title Page

Abstract

Introduction

Conclusions

References

Tables

Figures

◀

▶

◀

▶

Back

Close

Full Screen / Esc

Printer-friendly Version

Interactive Discussion



Soil erosion areas in the Blue Nile-Eastern Sudan

M. El Haj El Tahir et al.

Title Page

Abstract

Introduction

Conclusions

References

Tables

Figures

◀

▶

◀

▶

Back

Close

Full Screen / Esc

Printer-friendly Version

Interactive Discussion

Table 3. Classification report.

| Image | Average Accuracy | Overall Accuracy | Kappa Coefficient |
|----------------|------------------|------------------|-------------------|
| ASTER Mar 2006 | 93.37% | 82.21% | 0.82 |
| ASTER Dec 2006 | 86.79% | 75.20% | 0.75 |

Soil erosion areas in the Blue Nile-Eastern Sudan

M. El Haj El Tahir et al.

Table 4. Accuracy Statistics.

| | Class Name | Producer's Accuracy | User's Accuracy | Kappa Statistic |
|----------------|------------------|---------------------|-----------------|-----------------|
| ASTER Mar 2006 | Mountain | 88.24% | 97.83% | 0.97 |
| | Gully | 92.21% | 92.21% | 0.90 |
| | Flat | 96.30% | 92.31% | 0.83 |
| | Water | 70.00% | 87.50% | 0.87 |
| | Overall Accuracy | | 93.02% | |
| ASTER Dec 2006 | Mountain | 69.23% | 75.000% | 0.74 |
| | Gully | 87.00% | 85.294% | 0.78 |
| | Flat | 95.16% | 79.730% | 0.75 |
| | Water | 91.67% | 100.000% | 1.00 |
| | Overall Accuracy | | 89.00% | |

Title Page

Abstract

Introduction

Conclusions

References

Tables

Figures

◀

▶

◀

▶

Back

Close

Full Screen / Esc

Printer-friendly Version

Interactive Discussion



Soil erosion areas in the Blue Nile-Eastern Sudan

M. El Haj El Tahir et al.

[Title Page](#)

[Abstract](#)

[Introduction](#)

[Conclusions](#)

[References](#)

[Tables](#)

[Figures](#)

[I◀](#)

[▶I](#)

[◀](#)

[▶](#)

[Back](#)

[Close](#)

[Full Screen / Esc](#)

[Printer-friendly Version](#)

[Interactive Discussion](#)

Table 5. Classification report.

| Image | Average Accuracy | Overall Accuracy | Kappa Coefficient |
|----------------|------------------|------------------|-------------------|
| MODIS Mar 2006 | 77.18% | 61.85% | 0.40 |
| MODIS Dec 2006 | 81.02% | 63.82% | 0.20 |

Soil erosion areas in the Blue Nile-Eastern Sudan

M. El Haj El Tahir et al.

Table 6. Accuracy Statistics.

| | Class Name | Producer's Accuracy | User's Accuracy |
|----------------|------------------|---------------------|-----------------|
| MODIS Mar 2006 | Mountain | 94.118% | 80.000% |
| | Gully | 90.625% | 93.548% |
| | Flat | 89.744% | 89.744% |
| | Water | 75.000% | 90.00% |
| | Overall Accuracy | | 89.00% |
| MODIS Dec 2006 | Mountain | 91.21% | 80.01% |
| | Gully | 87.64% | 92.45% |
| | Flat | 85.73% | 89.94% |
| | Water | 72.60% | 91.40% |
| | Overall Accuracy | | 88.67% |

Title Page

Abstract

Introduction

Conclusions

References

Tables

Figures

◀

▶

◀

▶

Back

Close

Full Screen / Esc

Printer-friendly Version

Interactive Discussion



Soil erosion areas in the Blue Nile-Eastern Sudan

M. El Haj El Tahir et al.

Table 7. Estimated bi-temporal change in ASTER (60×60 km) scale during 2006 rainy season.

| Class | Area (%) | | | Area (km ²) | | |
|-----------|----------|--------|--------|-------------------------|---------|----------|
| | Mar | Dec | Diff | Mar | Dec | Diff |
| Gully | 42.1 | 50.87 | 8.77 | 538.5 | 650.677 | 112.177 |
| Flat Land | 46.6 | 34.63 | -11.97 | 596 | 442.907 | -153.093 |
| Mountain | 4.43 | 4.434 | 0.004 | 56.65 | 56.701 | 0.051 |
| Water | 6.87 | 10.066 | 3.196 | 67.9 | 99.488 | 31.588 |

Title Page

Abstract

Introduction

Conclusions

References

Tables

Figures

◀

▶

◀

▶

Back

Close

Full Screen / Esc

Printer-friendly Version

Interactive Discussion



Soil erosion areas in the Blue Nile-Eastern Sudan

M. El Haj El Tahir et al.

Table 8. Estimated bi-temporal change in the regional MODIS scale during 2006 rainy season.

| Class | Area (%) | | | Area (km ²) | | |
|-----------|----------|-------|--------|-------------------------|-----------|----------|
| | Mar | Dec | Diff | Mar | Dec | Diff |
| Gully | 33.1 | 39.65 | 6.55 | 10 467 | 12 538.26 | 2071.26 |
| Flat Land | 39.76 | 27.54 | −12.22 | 12 572 | 8708.07 | −3863.93 |
| Mountain | 21.3 | 21.3 | 0 | 6737 | 6737 | 0 |
| Water | 5.84 | 11.51 | 5.67 | 1845 | 3636.29 | 1791.29 |

Title Page

Abstract

Introduction

Conclusions

References

Tables

Figures

◀

▶

◀

▶

Back

Close

Full Screen / Esc

Printer-friendly Version

Interactive Discussion



Soil erosion areas in the Blue Nile-Eastern Sudan

M. El Haj El Tahir et al.

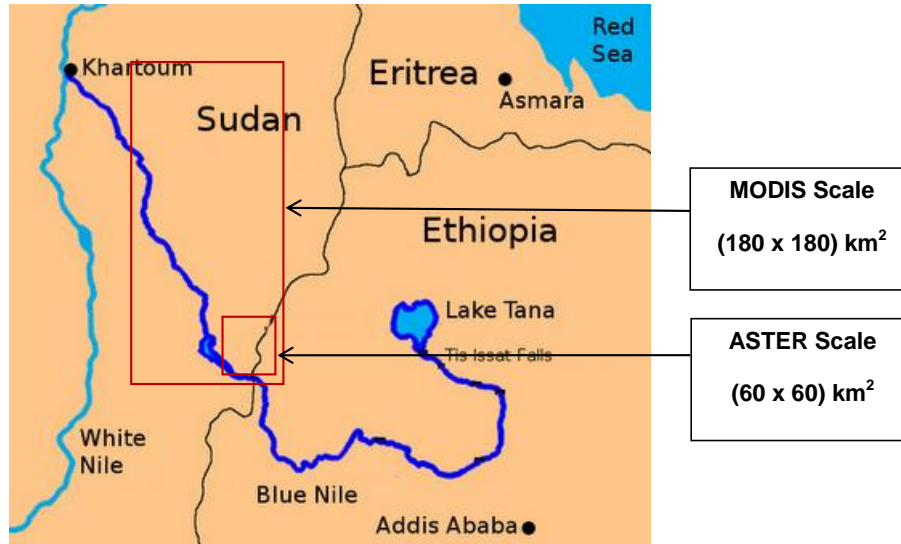


Fig. 1. Map of The Blue Nile State showing the study area. The area is divided into two scales: MODIS (180×180 km²) and ASTER (60×60 km²). The map is not to scale.

Title Page

Abstract

Introduction

Conclusions

References

Tables

Figures

◀

▶

◀

▶

Back

Close

Full Screen / Esc

Printer-friendly Version

Interactive Discussion



Soil erosion areas in the Blue Nile-Eastern Sudan

M. El Haj El Tahir et al.



Fig. 2. Erosion in *Khor Dunya* (photo taken January 2007).

Title Page

Abstract

Introduction

Conclusions

References

Tables

Figures

◀

▶

◀

▶

Back

Close

Full Screen / Esc

Printer-friendly Version

Interactive Discussion



Soil erosion areas in the Blue Nile-Eastern Sudan

M. El Haj El Tahir et al.

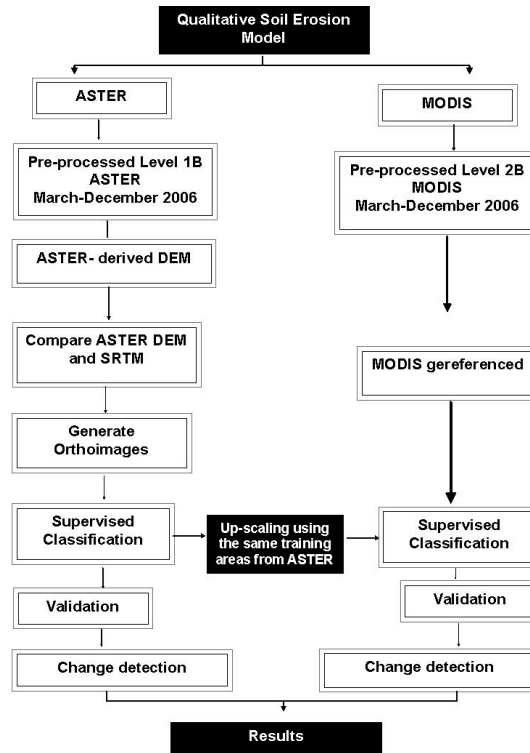


Fig. 3. Flow diagram summarising the methodology. On the left hand side are the steps involved using ASTER: generation of two DEMs from ASTER and their comparisons with SRTM; orthorectification of ASTER; stacking extra layers (namely addition of slope, aspect, DEM, and river flow network); supervised classification of ASTER. On the right hand side are those involving MODIS: selecting MODIS products (VNIR, NDVI, EVI); georeferencing; supervised classification using the same training areas imported from ASTER. Hence the change in area of eroded land between March and December 2006 is calculated on both MODIS and ASTER scales.

| | |
|--------------------------|--------------|
| Title Page | |
| Abstract | Introduction |
| Conclusions | References |
| Tables | Figures |
| ◀ | ▶ |
| ◀ | ▶ |
| Back | Close |
| Full Screen / Esc | |
| Printer-friendly Version | |
| Interactive Discussion | |



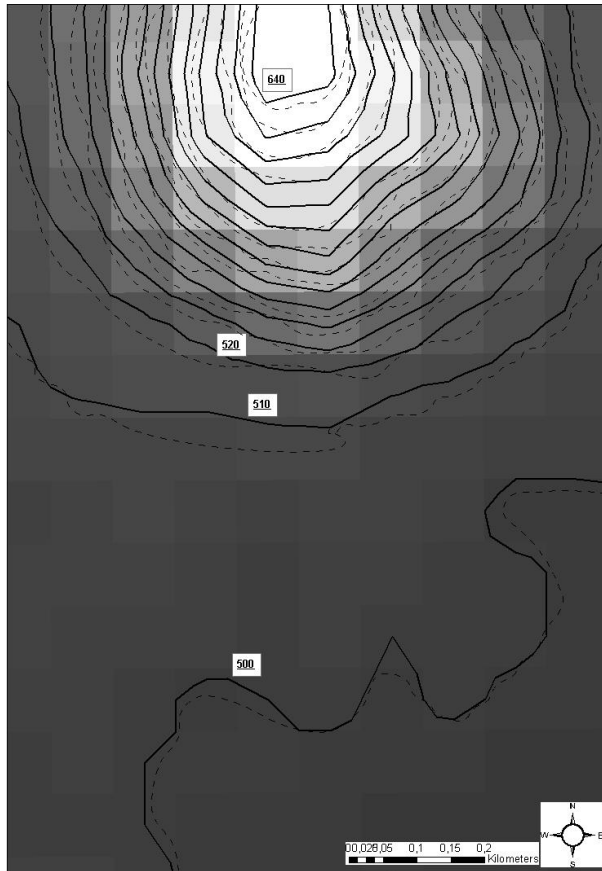


Fig. 4a. Elevation differences between SRTM DTM (solid line) and ASTER (18 December 2006) DEM (dotted line Fig. 4) and ASTER (30 March 2006) DEM (dotted line Fig. 5), superimposed on a hillshade of the SRTM in Ed Damazin area. The scenes mark a subset with a mix of moderate to high topography.

Soil erosion areas in the Blue Nile-Eastern Sudan

M. El Haj El Tahir et al.

Title Page

Abstract

Introduction

Conclusions

References

Tables

Figures

◀

▶

◀

▶

Back

Close

Full Screen / Esc

Printer-friendly Version

Interactive Discussion



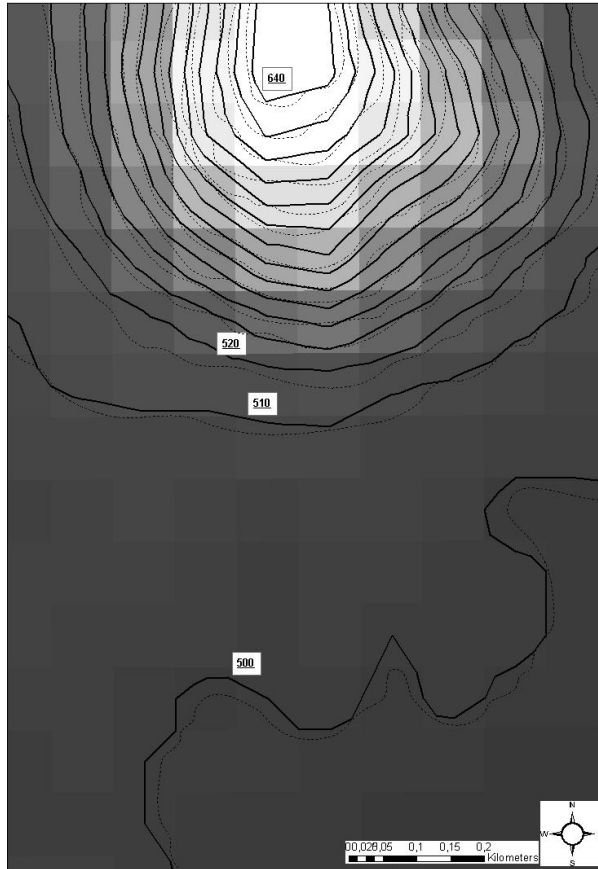


Fig. 4b. Continued.

Soil erosion areas in the Blue Nile-Eastern Sudan

M. El Haj El Tahir et al.

Title Page

Abstract

Introduction

Conclusions

References

Tables

Figures

◀

▶

◀

▶

Back

Close

Full Screen / Esc

Printer-friendly Version

Interactive Discussion



Soil erosion areas in the Blue Nile-Eastern Sudan

M. El Haj El Tahir et al.

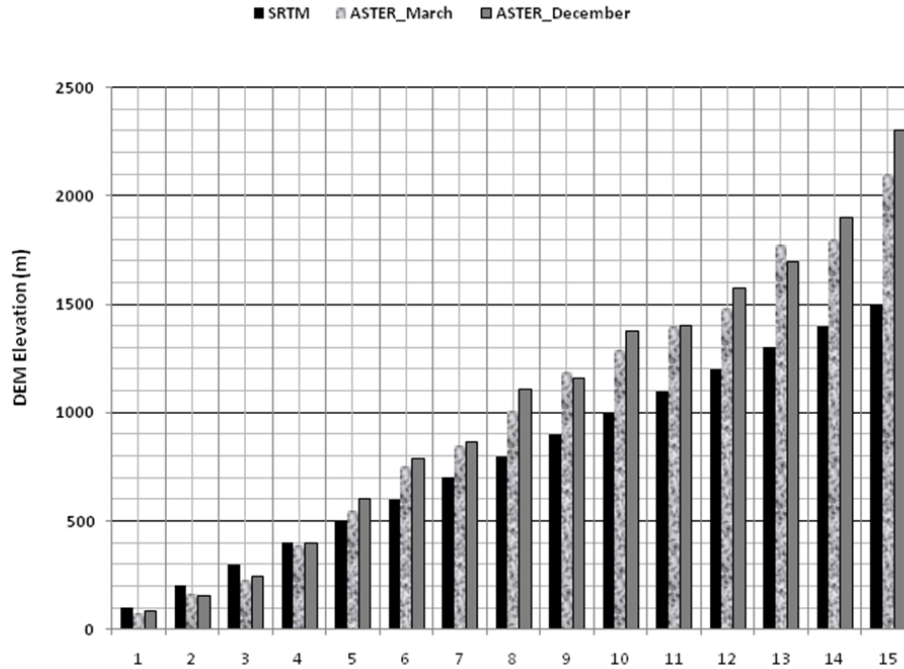


Fig. 5. Comparisons between SRTM and ASTER DEM.

Title Page

Abstract

Introduction

Conclusions

References

Tables

Figures

◀

▶

◀

▶

Back

Close

Full Screen / Esc

Printer-friendly Version

Interactive Discussion



Soil erosion areas in the Blue Nile-Eastern Sudan

M. El Haj El Tahir et al.

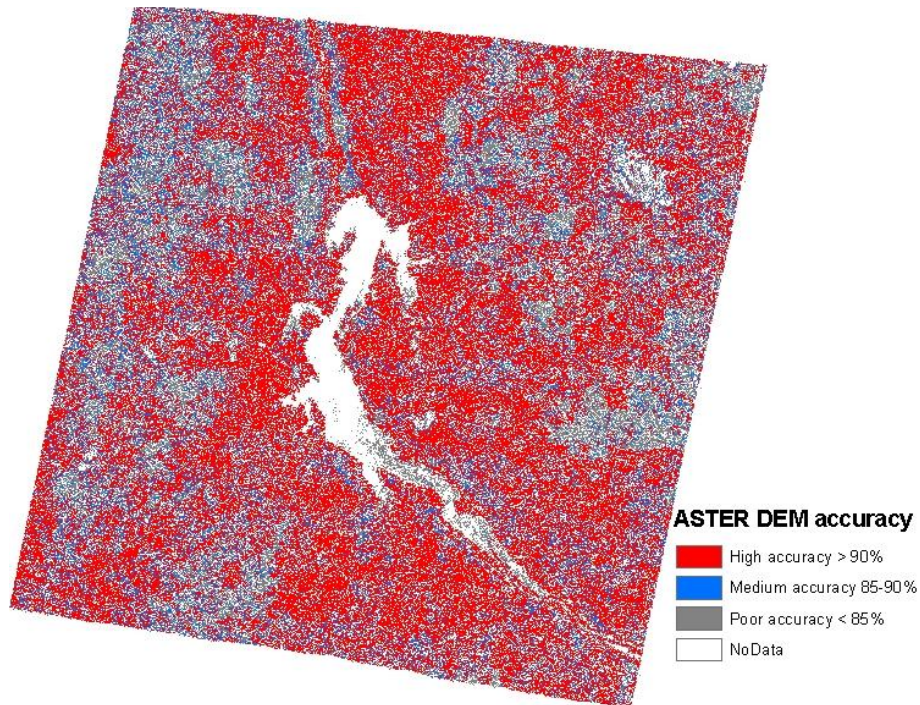


Fig. 6. Score channel: The reliability and accuracy of ASTER (18 December 2006) DEM.

Title Page

Abstract

Introduction

Conclusions

References

Tables

Figures

◀

▶

◀

▶

Back

Close

Full Screen / Esc

Printer-friendly Version

Interactive Discussion



Soil erosion areas in the Blue Nile-Eastern Sudan

M. El Haj El Tahir et al.

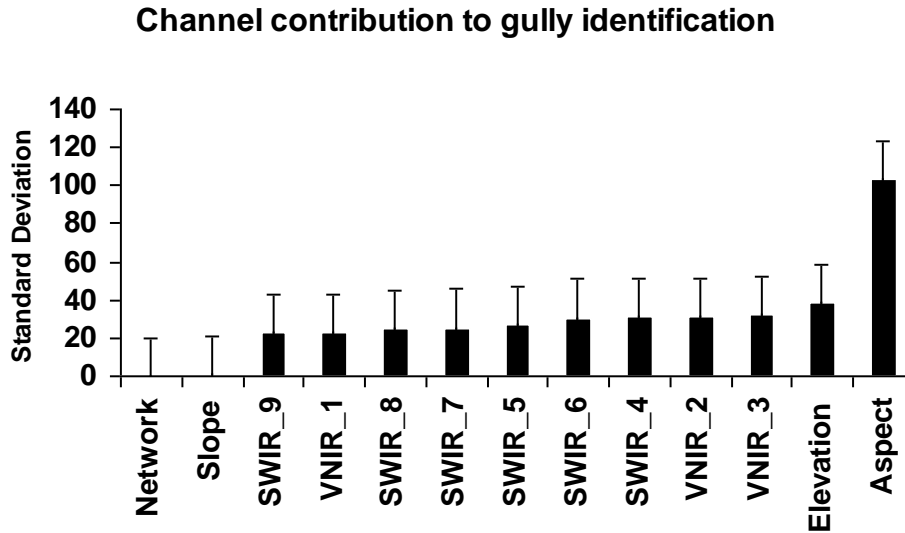


Fig. 7. Contribution of the different channels.

Title Page

Abstract Introduction

Conclusions References

Tables Figures

◀ ▶

◀ ▶

Back Close

Full Screen / Esc

Printer-friendly Version

Interactive Discussion



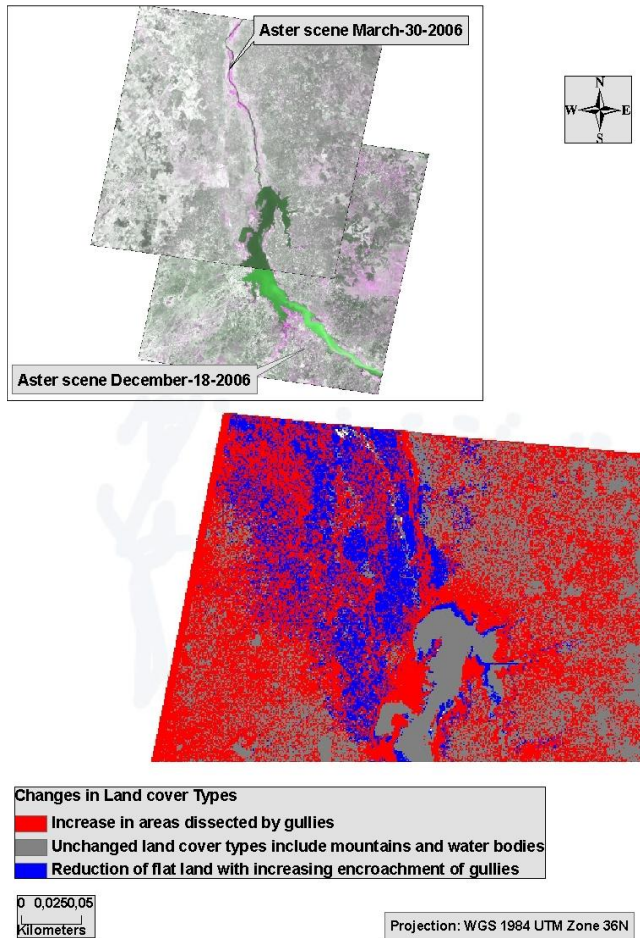


Fig. 8. Estimated bi-temporal changes in area of different land cover types between March and December 2006 using ASTER images.

Soil erosion areas in the Blue Nile-Eastern Sudan

M. El Haj El Tahir et al.

| | |
|--------------------------|--------------|
| Title Page | |
| Abstract | Introduction |
| Conclusions | References |
| Tables | Figures |
| ◀ | ▶ |
| ◀ | ▶ |
| Back | Close |
| Full Screen / Esc | |
| Printer-friendly Version | |
| Interactive Discussion | |

